Iranian Journal of Science and Technology, Transactions of Mechanical Engineering (2025) 49:445–461
https://doi.org/10.1007/s40997-025-00838-6

RESEARCH PAPER

Experimental and Numerical Investigations of Drag Reduction on a Van Using a Side Flap

Fatima-Zahra Hachimy[1] · Mohammed Aldheeb[2] · Ashraf A. Omar[1] · Waqar Asrar[2]

Received: 21 August 2024 / Accepted: 13 January 2025 / Published online: 24 February 2025

Abstract
The present study aims to examine the effect of a side flap on drag reduction and rolling moment stability as a passive flow control mechanism installed on a scaled square back van model, through both experimental and computational methods. The side flap significantly reduces drag, with the greatest decrease occurring when the flap is mounted at a 10° angle. The experimental work was carried out in a wind tunnel under low-speed conditions, with $Re = 5.1 \times 10^6$, and the aerodynamic force data were obtained through the utilization of a six-component force balance, while the simulation was performed using ANSYS-Fluent on a geometrically similar model at the same Reynolds number. Various flap mounting angles were evaluated to compare results and highlight the influence of the side flap on the wake area. The most advantageous angle was determined to be 10° resulting in up to 7% drag reduction. The optimal mounting angle was selected for the investigation of vehicle stability in crosswind conditions. The presence of the side flap has a notable effect on the drag reduction and stability of the van, resulting in a decrease in drag by about 7% and an improvement in rolling moment by 8% when subjected to a free stream flow yaw angle of 12°.

Keywords Drag reduction · Stability · Van · Crosswind · Wind tunnel testing · CFD

1 Introduction

There are numerous compelling reasons why reducing fuel consumption in road vehicles is crucial. High fuel usage has a detrimental influence on air quality and accelerates climate change by producing large amounts of air pollution and greenhouse gas emissions. Second, reducing fuel consumption has financial advantages. Road cars that are efficient help keep fossil fuel supplies available for a longer period of time for future generations (Ehsani et al. 2016).

Depending on the kind of vehicle, its design, and its speed, the contribution of aerodynamics can vary greatly. At high speeds, aerodynamic drag often contributes significantly to vehicle's fuel consumption. Aerodynamic drag can account for 30–50% of the overall fuel consumption for the majority of automobiles moving at highway speeds (Hucho and Sovran 1993). This indicates that aerodynamic considerations may account for up to half of the energy needed to overcome resistance. It's crucial to keep in mind, though, that bigger cars like SUVs, trucks, and commercial vehicles may have a greater proportion. To lessen this aerodynamic drag and improve fuel economy, automakers and engineers continuously improve the aerodynamic shape of automobiles as well as incorporate passive drag reduction devices.

The aerodynamic drag is mainly pressure drag, and skin friction drag. For road vehicles, the pressure drag accounts for about 80% of the total aerodynamic drag and it is highly suggested to focus on its reduction (Wood 2004). The reduction can be achieved by implementing flow control mechanisms to modify the flow structure around the vehicle. Several researches have been conducted to study both passive flow control techniques (Altaf et al. 2014, 2022; Tian et al. 2017a) and active techniques (Jahanmiri and Abbaspour 2011; Heinemann et al. 2014; Cerutti et al. 2020). While the passive control approach is fairly successful and has drawn study interest, active control remains a very sophisticated

✉ Ashraf A. Omar
ashraf_omar@uir.ac.ma

[1] School of Aerospace and Automotive Engineering, LERMA Lab, International University of Rabat, Sala El Jadida 11100, Morocco

[2] Department of Mechanical Engineering, Faculty of Engineering, International Islamic University Malaysia, PO Box 10, Kuala Lumpur 50728, Malaysia

and complex control that requires extra energy inputs and largely feedback management. Additionally, the passive procedures are easily adaptable to other structures, particularly the bluff shape vehicles that are the primary focus of this work.

One of the employed active methodologies is the method of steady blowing. The impact of steady blowing was examined by Heinemann et al. through experimental studies on a real car model (Heinemann et al. 2014) at three distinct positions. Their findings revealed a 5% reduction in rear axle lift with a 1% change in the coefficient of drag (CD). Another study assessed the steady blowing efficacy at various angles on the wake structure applied on the roof trailing edge of a simplified ¼ scale square back vehicle (Mestiri et al. 2014). The steady suction effectiveness has also been assessed using a simplified fastback car model through both numerical and experimental methods. This technique has demonstrated the capability to mitigate the separation occurring at the rear window and decrease drag up to 17% (Kourta and Mechanics 2012). The effectiveness of using a pulsed jet to suppress the recirculation at the rear slant of an Ahmed body was studied experimentally for a 25° slant angle. Results indicated that a maximum drag reduction ranging from 6 to 8% could be attained depending on the specific jet exhaust parameters and geometric configurations, which exhibit varying degrees of sensitivity to the applied forcing conditions (Joseph et al. 2012).

Regarding the passive flow control technique, several researches have been conducted to investigate its effectiveness. By altering the underbody's form and diverting exhaust gas to the back of the car, Hassan et al. (Hassan et al.) highlighted a number of characteristics of drag reduction strategies. Consequently, underbody modification techniques were able to reduce drag by up to 22%, while exhaust gas redirection reduced drag by up to 9%. Three delta-shaped vortex generators were used in the investigation, and they were placed at the roof end of the sedan vehicle model, which is where the flow separation starts from the automobile's exterior. According to the experimental findings, the lift and drag coefficients were reduced by 2.55% and 4.53%, respectively. Selvaraju et al. (Ponnusamy et al. 2016) also conducted an experimental aerodynamic analysis and numerical prediction on a typical car model to estimate drag force and pressure distribution characteristics in the mid plane of the car model. The scientists came to the conclusion that boundary layer thickness had a bigger influence on constructing the vortex generator as an aerodynamic add-on device and that the drag coefficients derived through theoretical and experimental approaches were in close agreement with one another. Mariotti et al. showed that using curved grooves on the boat tail surface significantly affected the aerodynamics, reducing it by 9.7% (Mariotti et al. 2019). In an experimental research, Lorite-Diez et al. discovered a 10% reduction in drag when using rear cavities (Lorite-Díez et al. 2020). The use of altered automobile designs, such as a tapered rear upper body on the top and sides, to reduce aerodynamic drag has been investigated by Howell et al. (Howell et al. 2013). They used PIV to visualize the wake flow and distributed pressure and looked at force reduction on an Ahmed body that was remodeled and had base cavities.

Compared to the private automotive sector, the commercial vehicle business discourages the regular introduction of new models due to distinct market dynamics. Since new models take longer to create, produce, and bring to the market than new car models, they are likely to stay on the market for a longer period of time. Furthermore, a lot of money is spent on trucks and buses, particularly in developing countries, because of the function they provide and the fact that they are used widely around the world. If these vehicles' aerodynamic drag is decreased, they may save a lot of money by consuming less fuel. Numerous studies have looked into techniques to lower the aerodynamic drag of commercial vehicles, such as trucks, buses, and vans, which typically have square back bluff shape. To regulate the forebody flow of heavy trucks, a variety of flow control devices have been devised, including the cab deflector (KR Cooper 2003; Lazăr 2021), front spoiler (Hyams et al. 2011), cab side extender (Martini et al. 2011), and cab roof fairing (Kim et al. 2017). To regulate underbody flow, side skirts—which are typically made of straight panels that curtain the region beneath the front and rear wheels—are frequently used (Hwang et al. 2016). By using flaps on the Ahmed body model, Jie tian et al. were able to reduce drag by up to 21.2% through numerical research (Tian et al. 2017b). By looking at the installation of an elliptical flap on a MAN TGX truck, Altaf et al. were able to obtain a drag reduction of almost 11% (Altaf et al. 2014). Numerous passive flow control strategies, such as porous medium (Sadeghipour et al. 2020), the use of a rough surface (Kumar Shaw et al. 2020) and the use of dimples (Wong et al.) have been employed.

Ensuring vehicle stability in crosswind conditions is crucial for sustaining secure and predictable driving experiences. Lateral air movements, known as crosswinds, can provide significant challenges in their management, particularly when operating at high speeds. An impeccably engineered and sturdy vehicle effectively withstands the destabilizing forces generated by crosswinds, hence minimizing the risk of unexpected lane deviations and enhancing overall safety. Manufacturers employ sophisticated aerodynamic engineering and rigorous testing methods, including wind tunnel simulations and real-world trials, to enhance a vehicle's stability profile. The focus on crosswind stability

not only enhances driver confidence and comfort, but it is also a vital factor in meeting the stringent safety standards and regulations of the automotive industry.

Vans are often regarded as one of the most common types of road vehicles. They are utilized for both the movement of humans and freight, among other purposes. They are employed by both large industries and small firms. According to prior study(Hachimy et al. 2023), adding a side flap to a van model's back has significantly reduced drag by 11%. A numerical study employing the Taguchi test design approach was performed to optimize the side flap design and achieve maximum drag reduction. The optimal design was a convex flap with an inclination angle of 10°.

To the best of the authors' knowledge, the experimental investigation of a side flap as an add-on device implemented to a van model was not investigated so far. Moreover, to date, no empirical investigation has been undertaken to assess its influence on roll moment stability when subjected to crosswind conditions. The primary aim of the present study is to experimentally and computationally examine the impact of a lateral flap on a scaled model of a van, as well as its efficacy in mitigating the effects of crosswinds. The findings section analyses and evaluates the effect of a lateral flap on the drag and rolling moment of a van obtained for free stream yaw angles, ranging from 0° to 12°.

2 Experimental Apparatus and Method

2.1 Wind Tunnel Testing

Wind tunnel testing is an essential part of the process of developing and designing automobiles since it gives researchers and engineers vital knowledge about how aerodynamically efficient they operate. For the present work, wind tunnel experiment is carried out at the International Islamic University of Malaysia's aerodynamic Lab in a small Tecquipment open circuit wind tunnel AF1300. The AF1300 wind tunnel is used in numerous research investigations (Ali 2022; Mohammadi and Taleghani 2012) and it is equipped with a test section that has dimensions of 305 mm in height, 305 mm in width, and a length of 600 mm. Additionally, the maximum velocity attained within this wind tunnel is 36 m/s. The wind tunnel is factory calibrated. The wind speeds were measured using a pitot-static tube and U tube manometer. The experiment is carried out at a constant wind speed of 30 m/s, and Reynolds number of 5.1×10^6 based on the model length.

A six-component external force balance DARCS XB6C-200 is used to measure the aerodynamic forces on the vehicle model and has an uncertainty of 0.2% FS. The Balance details are as follows: Turn table diameter 200 mm, Load range: Axial Force: $\pm$ 220 N, Side Force: $\pm$ 220 N, Normal Force: $\pm$ 440 N, Rolling moment: $\pm$ 11Nm, Pitching moment: $\pm$ 11Nm, Yawing moment: $\pm$ 5.6Nm, Control: Computer controllable with DARCS.

The data obtained from three independent observations are statistically averaged to calculate the drag force along the wind direction (X-axis). The model is attached to the six-component force balance in the wind tunnel floor turning table as shown in Fig. 1(b) and the schematic in Fig. 1(d). The uncertainty in all measurements is $\pm$ 0.2% FS.

The turning table is used to measure the aerodynamic performance at different yaw angles. The yaw angle is the angle between the vehicle's path and the direction of airflow. The yaw angle used in the current study ranges from 0° to 12° with an increment of 2°. Considering that vehicles at high speeds never experience a larger yaw angle (Cheng et al. 2019), the maximum yaw angle was set at 12°. The wind tunnel's integrated turntable was used to attach the model so that the yaw angle could be adjusted.

The aerodynamic drag coefficient C_D and the rolling moment coefficient C_M are obtained directly from the six-component force balance based on the entered wind tunnel speed, model frontal area, wind tunnel air density, and viscosity.

2.2 Vehicle Model

This study investigates the impact of different side flap configurations on aerodynamic drag and stability. A simplified van model, as shown in Fig. 2, is employed for this purpose. The model that is being utilized in this study is a scaled-down version of the basic driven vans. Scaling is employed in wind tunnel experimentation to examine the aerodynamic characteristics and efficacy of large structures within a regulated and cost-effective environment. Scaled experimentation permits the analysis of aerodynamic metrics such as lift, drag, stability, and flow dynamics during the initial design stages, enabling incremental modifications prior to the construction of full-scale prototypes. While scaling offers a pragmatic and economically viable method for aerodynamic analysis, it is accompanied by inherent constraints. Variations in Reynolds numbers between scaled models and their full-scale counterparts frequently result in inaccurate flow behavior, exemplified by the transition from turbulent to laminar flow in certain regions. Disparities in material properties and nonlinear dynamics, such as vortex shedding and unsteady flow conditions, further exacerbate the challenges associated with the extrapolation of experimental results. These limitations, in conjunction with the challenges of achieving ideal similitude, necessitate the implementation of corrections and computational modifications, which subsequently introduce assumptions and potential inaccuracies. Despite these obstacles, meticulous

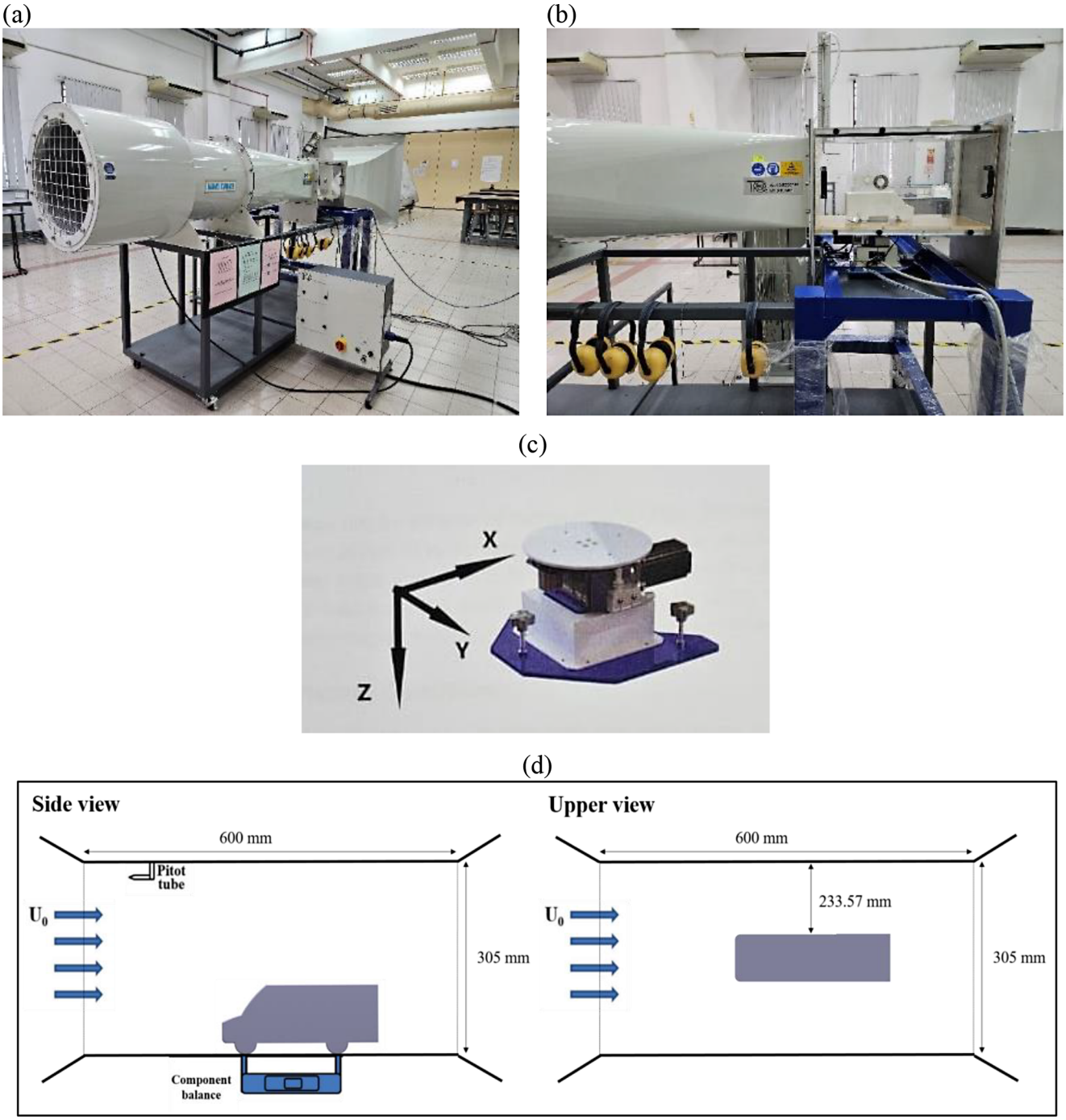

Fig. 1 (**a**) Subsonic wind tunnel (**b**) Test section (**c**) Turning table (**d**) schematic of test section and external balance

experimental design can significantly alleviate these limitations, thereby ensuring that scaling continues to serve as a fundamental component of wind tunnel experimentation.

In the subsequent investigation, many simplifying assumptions were employed. Geometry plays a crucial role in aerodynamics, as the frontal area of an object is primarily responsible for generating the majority of the aerodynamic drag, especially for bluff bodies. Consequently, while developing vans, the underbody and cabin shape are not given concern (Leuschen and Cooper 2009). The geometry of the tyre, which was intentionally designed to possess a circular profile with a shallow rectangular section, is the focus of the second simplification.

The vehicle model was reduced in size to 1/28 scale for the wind tunnel testing in order to keep the blockage ratio between the model and the test section's cross-sectional

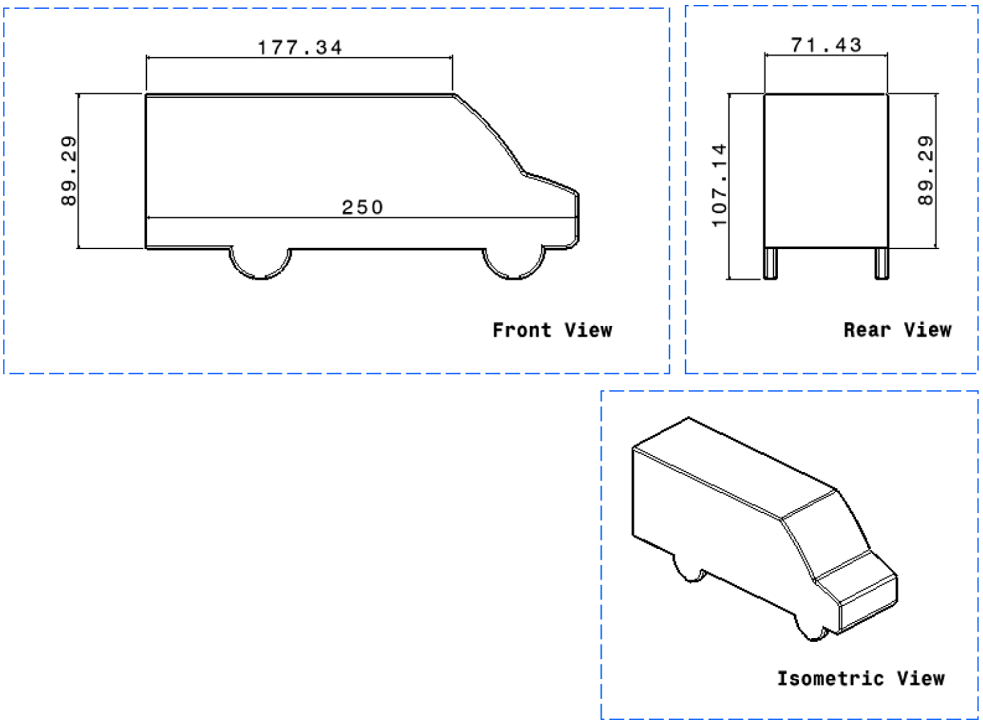

Fig. 2 Scaled van model dimensions (in mm)

area below 10%. This blockage factor is calculated by dividing the test object's frontal area by the test section's cross-sectional area (Haque et al. 2016), which is around 8% for the current study. The greatest blockage ratio required to produce reliable findings is 10% according to Barlow et al. (Barlow et al. 1999). Meanwhile, West and Apelt (West and Apelt 1982) found that when the blockage ratio is less than 6%, the effects of model blockage on the observed pressure distribution and drag coefficient are insignificant. However, the recommended side flap's relative advantages over the regular vehicle model are unchanged since their drag coefficients are both impacted by an almost similar blockage ratio. The model was built using a 3D printer. The material employed in the three-dimensional printing process is Polylactic Acid (PLA), which is classified as a thermoplastic filament. The three-dimensional printer constructs the models incrementally by depositing successive layers. The interlayer spacing for the printed model is precisely 0.1 mm. Subsequently, the surface of the model was refined utilizing sandpaper. The final grade of sandpaper employed was 400 grit/mm². Figure 3(a) shows the printed van model with a length of 250 mm, height of 107.14 mm, and width of 71.43 mm. The model is printed in two sections to retain the forebody unchanged and to print multiple rear configurations with 5 varied side flap angles, as illustrated in Fig. 3(c). Figure 3(b) shows the design sketch of the side flap, when Fig. 3(d) illustrates the top view sketch of the different rear parts with the different side flap angles.

3 Numerical Simulation

3.1 Turbulence Model

Numerous sectors have found great success with numerical simulation as a methodology. The automobile sector embraced it to solve and forecast flow behavior over cars and to provide designers with a trial ground before going into production. Computational fluid dynamics (CFD) simulation is used to carry out the numerical work reported in this paper. ANSYS-Fluent is the software utilized for the analysis of the investigation. The three-dimensional flow around the vehicle is considered steady and incompressible. Some studies focused on comparing the turbulence models in predicting the aerodynamic characteristics of air vehicles (Somashekar 2021). Considering its effectiveness in forecasting the flow behavior, the Shear Stress Transport (SST) model, which is based on the blending functions of both the k-ε and k-ω turbulence models, is selected for the analysis of the turbulent flow over the vehicle model. The SST model is a hybrid of the k-ε and k-ω turbulence models, which enhances its predictive accuracy (Hachimy et al. 2022). The Shear Stress Transport (SST) turbulence model parameters were set to their default values in ANSYS-Fluent (ANSYS-FLUENT). The following is the formulation of the SST turbulence model and more details can be found in reference (Menter et al. 2003).

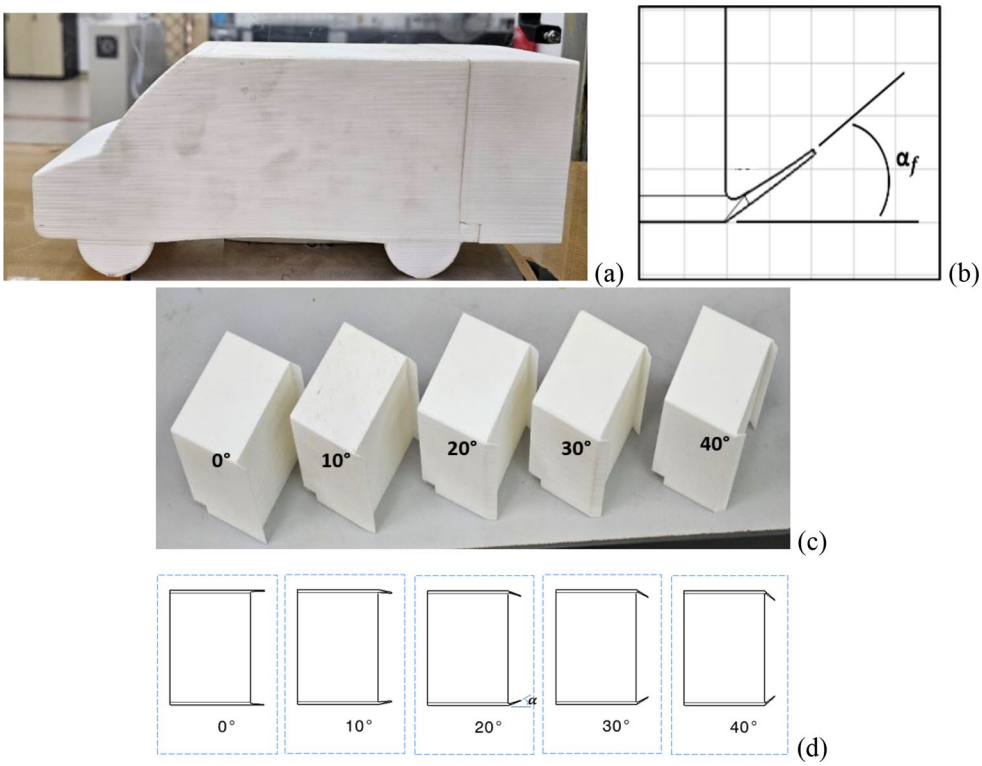

Fig. 3 (**a**) Scaled van model (**b**) Sketch of the side flap and flap angle (**c**) Rear parts with different side flap angles (**d**) Top view sketch of the rear parts with side flaps

$$\frac{\partial(\rho k)}{\partial t}+\frac{\partial(\rho U_i k)}{\partial x_i}=\widetilde{P}_k-\beta^*\rho k\omega+\frac{\partial\left[(\mu+\sigma_k\mu_t)\frac{\partial(k)}{\partial x_i}\right]}{\partial x_i} \tag{4}$$

$$\frac{\partial(\rho\omega)}{\partial t}+\frac{\partial(\rho U_i\omega)}{\partial x_i}=\alpha\rho S^2-\beta\rho\omega^2+\frac{\partial\left[(\mu+\sigma_\omega\mu_t)\frac{\partial(\omega)}{\partial x_i}\right]}{\partial x_i}+2(1-F_1)\rho\sigma_{\omega 2}\frac{1}{\omega}\frac{\partial k}{\partial x_i}\frac{\partial\omega}{\partial x_i}$$

The definition of the blending function F_1 is as follows:

$$F_1=tanh\left\{\left\{min\left[max\left(\frac{\sqrt{k}}{\beta^*\omega y},\frac{500\gamma}{y^2\omega}\right),\frac{4\rho\sigma_{\omega 2}k}{CD_{k\omega}y^2}\right]\right\}^4\right\} \tag{5}$$

The SST model utilizes a production limiter, which is defined as follows, in stagnation zones to prevent the build-up of turbulence.

$$P_k=\mu_t\frac{\partial U_i}{\partial x_j}\left(\frac{\partial U_i}{\partial x_j}+\frac{\partial U_j}{\partial x_i}\right)\rightarrow\widetilde{P}_k=min(P_k,10.\beta^*\rho k\omega) \tag{6}$$

The constants for this model are computed via $\alpha=\alpha_1F+\alpha_2(1-F)$ and they are as follow: $\alpha_1=5/9$, $\alpha_2=0.44$, $\beta^*=0.09$ and $\sigma_{\omega 2}=0.856$.

3.2 Setup and Meshing

The CAD model used in the numerical simulation has the same dimensions as the wind tunnel model. Figure 4(a) depicts the computational domain employed for conducting the simulation. The dimensions of the flow domain in the x, y, and z directions are 13 times the length of the van model (3 times the length from the inlet and 10 times the length from the outlet), 5 times the width of the van model, and 3.5 times the height of the van model, respectively. A tetrahedral mesh cell is generated with a min size of 0.002 m. Subsequently, a mesh refinement was implemented in close proximity to the surface of the body. The mesh utilized for the current study model is depicted in Fig. 4(d). Two distinct bodies of influence were applied around the van body to generate the mesh clustering in the adjacent areas. 10 inflation layers with first layer thickness of 0.0005462 m are created around the model wall to obtain a y+value of 50. The computational domain consists of 6,537,563 cells. The mesh is shown in Fig. 4. Regarding the boundary conditions, the upper face and both sides of the computational domain were designated as symmetrical. The ground and the surfaces of the vehicle were designated as walls with the no-slip condition. Various numerical simulations were conducted for the baseline model using various mesh sizes, and the appropriate mesh coarseness value was selected for further simulations. Table 1; Fig. 5 display

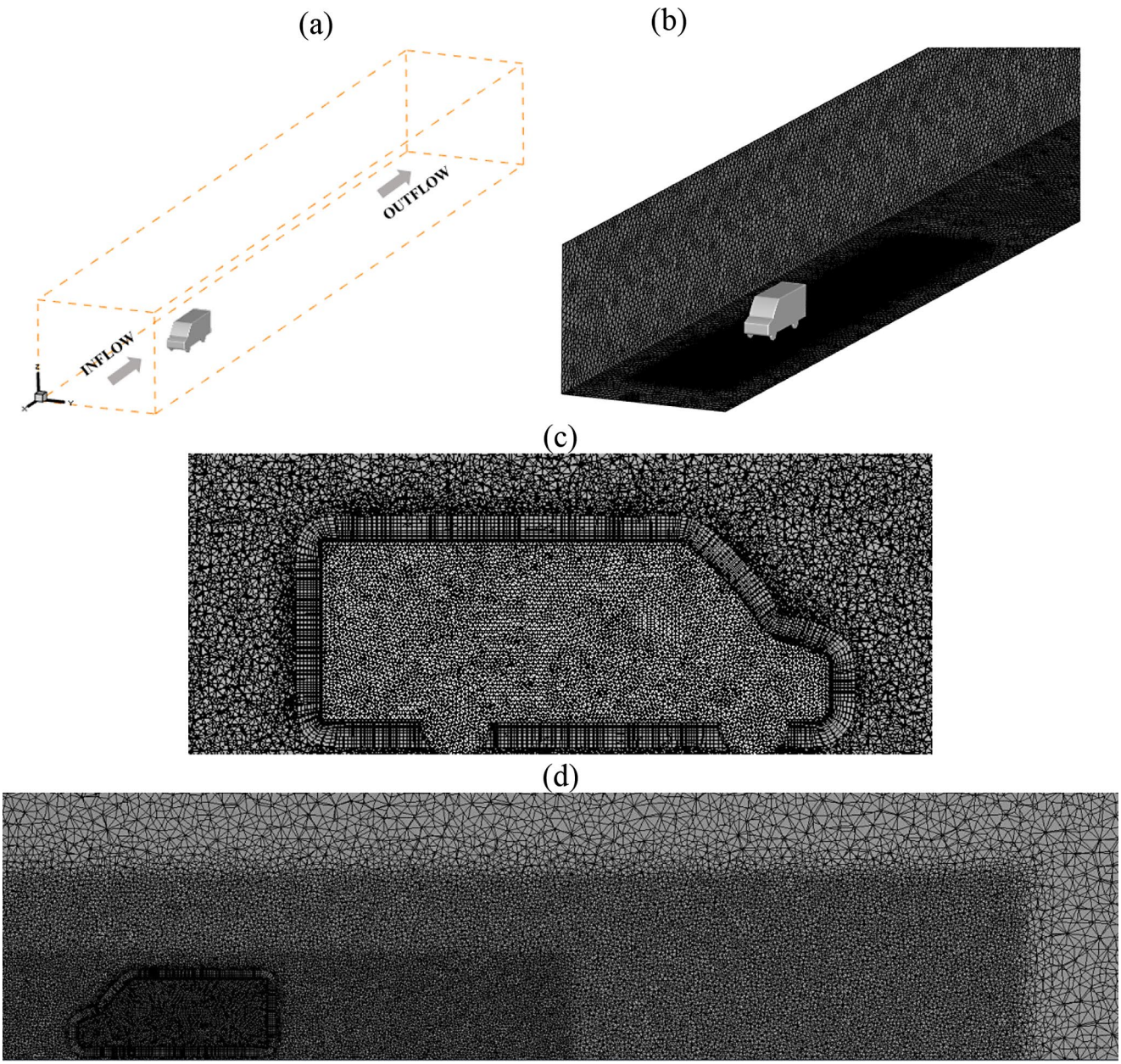

Fig. 4 (**a**) Computational Domain (**b**) Unstructured Mesh (**c**) Inflation layers around the body model (**d**) Mesh with clustering around the vehicle model

Table 1 Mesh grid independence

Mesh	No. of cells	Drag coefficient
Coarse	4,257,662	0.4174
Medium	5,828,564	0.3940
Fine	6,537,563	0.3974
Extra-fine	7,765,354	0.3972

the test results and graph, respectively. The mesh size chosen for this investigation is 'fine'. Table 2 displays the different parameters utilized for meshing.

4 Results and Discussion

4.1 Effect of Side Flap on Drag Reduction

The first section of the study revolves on analyzing the drag reduction device that has been included into a 1/28 scaled baseline model. The data sampling using the external force balance was performed thrice, and the final reported value is the average outcome. Table 3 displays the data sampling

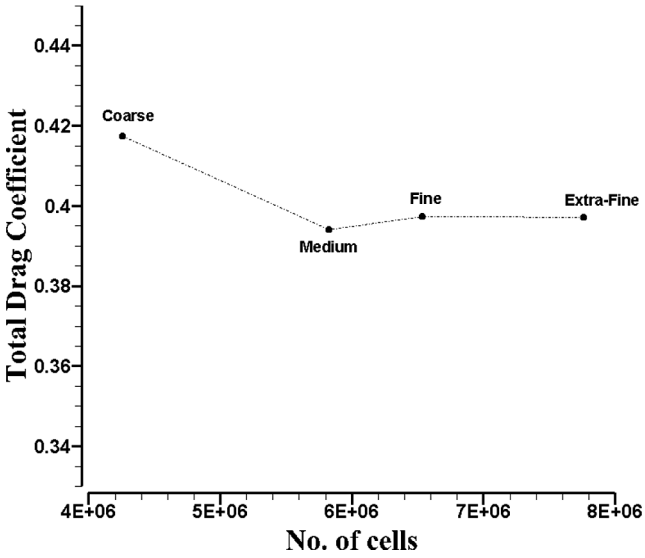

Fig. 5 Grid Independence graph

Table 2 Mesh parameters

Mesh Properties	Parameter
Max. number of inflation layers	10
First layer thickness (in m)	0.0005461859
Minimum element size (in m)	0.002
Growth rate	1.2
Total no. of elements	6,537,563

Table 3 Experimental data sampling for the drag, roll moment and yaw coefficients

	C_D	$C_{M_{roll}}$	$C_{M_{yaw}}$
1st reading	0.5070	0.00734	0.01773
2nd reading	0.5050	0.00426	0.00927
3rd reading	0.5050	0.00381	0.01044
Av	0.5056	0.00514	0.01248

and the ultimate averaged result for the total drag coefficient, roll moment coefficient, and yaw moment coefficient of the baseline. The average drag coefficient obtained is 0.505, while roll moment and yaw moment coefficients are 0.00514 and 0.01248, respectively.

The results of both experimental and simulation model are shown in Table 4 for different types of flaps configurations /angles compared to the baseline model. Implementing a side flap to the baseline model has a significant impact on the aerodynamic drag and mainly the pressure drag resulted from the generated wake area. The 0° side flap resulted in a drag reduction of about 3%. The drag reduction increases to 7.84% for a side flap with 10° inclination. This can be related to the fact that the side flap delays the separation of the side flow and redirects the flow within a 10° angle resulting in a smaller wake area. Coming to the 20° side flap, the drag coefficient increases back, and the drag reduction is nearly 3%. For both 30° and 40° side flap angles, the reduction of the aerodynamic drag decreases to around 3%. The 10° side flap is the best configuration achieving a maximum drag reduction of about 7%, with the remaining inclination angles contributing to a lesser extent. Concerning the numerical results, the computed drag coefficient is 0.397, exhibiting a minor deviation from the experimental measurement. Discrepancies in the drag coefficient between numerical analyses and experimental observations were identified, which may be attributable to variations in turbulence modeling, grid refinement, or boundary conditions within numerical simulations, in addition to potential measurement inaccuracies or test section interferences in experimental configurations. The study found that the greatest noticeable reduction in drag occurs when the side flap angle is set at 10°, based on both experimental and numerical tests conducted on various flap installation settings. This is consistent with the parametric analysis reported in the prior research study (Hachimy et al. 2023). Figure 6 represents the plot of the drag coefficient results of the different side flap configurations, for both the experiment and the numerical simulation. The experimental and numerical findings demonstrate a consistent agreement with the drag reduction rate, irrespective of the variations in the drag coefficient values. Empirical evidence supports the assertion that the 10° angle arrangement is optimal for doing in-depth research on crosswind phenomena.

In order to delve deeper into the process of reducing pressure drag, many scenarios were analyzed by comparing their velocity contours and pressure distributions. The purpose of including a side flap in this study is to mitigate the aerodynamic drag by attenuating the vortices generated at the posterior section of the model. The square back van type was included in this investigation due to its substantial wake area. Figures 7 and 8 display the velocity and pressure contours on the horizontal plane for the

Table 4 Drag coefficient results for different side flap angles (experimental and numerical)

Baseline		Side Flap				
Experimental	Numerical	Angle	Experimental	Reduction	Numerical	Reduction
0.51	0.3974	0°	0.49	3.92%	0.370	6.89%
0.51	0.3974	10°	0.47	7.84%	0.362	8.68%
0.51	0.3974	20°	0.49	3.92%	0.364	8.40%
0.51	0.3974	30°	0.49	3.92%	0.381	4.10%
0.51	0.3974	40°	0.49	3.92%	0.382	3.88%

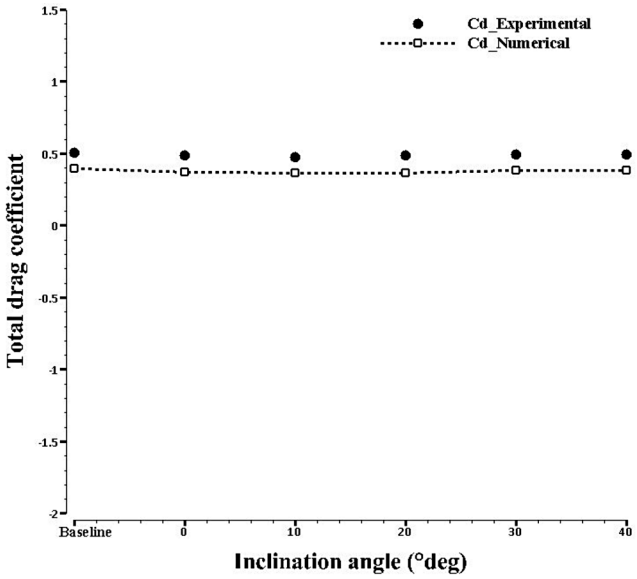

Fig. 6 Experimental vs. Numerical results

baseline configuration and the model equipped with a side flap positioned at various angles α (0°, 10°, 20°, 30°, and 40°), respectively.

The contour maps of the baseline model indicate that the wake region behind the model is extensive and characterized by a low-pressure zone. The side flap, located at the back of the model, had a substantial impact on the wake area. When the mounting angle is set at 0°, the longitudinal vortex is diminished, while the pressure behind it experiences a minor drop. This can be shown in Figs. 7 and 8, where the contour color shades indicate these changes. As the degree of inclination grew, the wake region experienced a decrease in strength and a minor displacement from the surface of the model. When the flap was positioned at an optimal inclination angle of 10°, the intensity of the vortex behind it was significantly reduced. This conclusion is consistent with the drag coefficient findings mentioned earlier. The rise in the drag coefficient is attributed to the formation of a low-pressure zone on the surface of the side flap. The magnitude of this zone and its strength grow as the inclination angle rises, as seen in Fig. 8.

4.2 Effect of Side Flap on the Flow Behavior in Crosswind

Regardless of the presence of a side flap, the yaw angle will consistently have a detrimental effect on the drag coefficient (C_d), side force coefficient (C_{side}), and moment coefficient (C_M). However, in the absence of the side flap, the impact of the yaw angle on the two force coefficients deteriorates significantly beyond a yaw angle of 6°, as seen by the sudden increase in the two force coefficients. The optimum side flap configuration with 10° inclination angle is the subject of the study under crosswind compared to the baseline model. The experimental findings for the drag and side force coefficients at various yaw angles ranging from

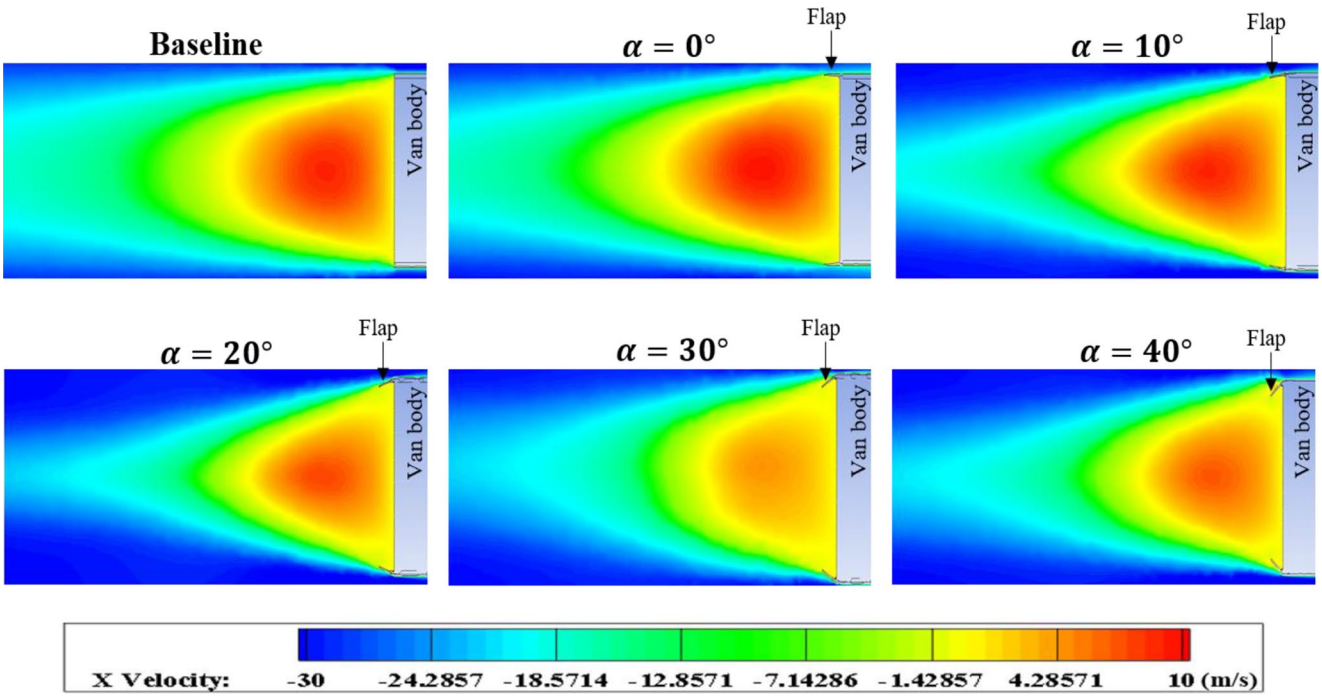

Fig. 7 Effect of flap inclination angles (α) on the x-velocity component at z=0.05 m at the rear of the van model shown as Horizontal-plane velocity contours

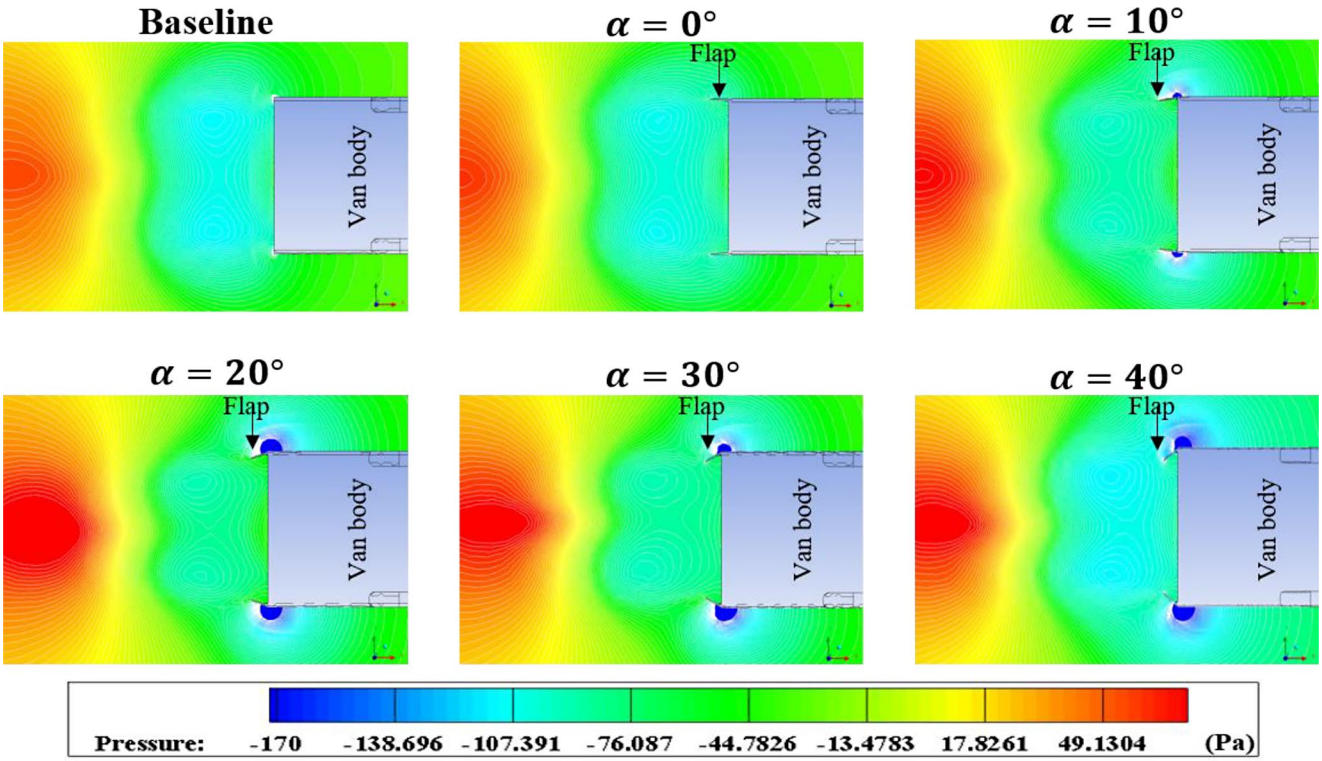

Fig. 8 Effect of different flap inclination angles on pressure shown as horizontal-plane pressure contours at the rear back of the van model for the at z = 0.05 m

Table 5 Experimental results of the total drag coefficient and the side force coefficient at a Re= 5.1×10^6

	Force coefficients					
Angle (°deg)	$C_{d_{baseline}}$	$C_{d_{modified}}$	**Reduction**	$C_{side_{baseline}}$	$C_{side_{modified}}$	**Reduction**
0	0.51	0.47	7.84%	0.0546	0.0715	30.89%
2	0.5113	0.5037	1.50%	0.1444	0.1433	0.78%
4	0.5520	0.5287	4.23%	0.2926	0.2716	7.17%
6	0.6040	0.5810	3.81%	0.4426	0.4197	5.17%
8	0.6467	0.6247	3.40%	0.5637	0.5413	3.98%
10	0.7090	0.6833	3.62%	0.6997	0.6700	4.24%
12	0.7683	0.7120	7.33%	0.7933	0.7260	8.48%

0° to 12° with a 2° increment are shown in Table 5. The outcomes of both the original and the altered model, which includes the addition of a side flap, are provided and compared. Table 6 presents the experimental data for the roll moment and the yaw moment. The relationship between the rise in yaw angle and the resulting force and moments exerted on the vehicle is evident. All the coefficients exhibit a significant increase. The addition of the side flap to the model has a substantial impact on the vehicle's stability. The drag coefficient experienced a reduction of 7% when the yaw angle reached 12°. Similarly, the coefficient of side force increased by 8.48% and the coefficient of roll moment increased by 8.70%. The collected data also included the values for the yaw moment. The yaw moment coefficient has a positive correlation with yawing. Nevertheless, including the side flap does not necessarily result in a decrease. The coefficients for yaw moment exhibited a little upward trend. This can be attributed to the fact that the side flaps are affixed to the rear end, so augmenting the overall length of the vehicle.

Figure 9 illustrates the changes in the drag coefficient (a), side force coefficient (b), roll moment coefficient (c), and yaw moment coefficient (d) as the yaw angle varies for both the baseline and modified model. The shown findings are derived from the experiment. Attaching the side flap to the vehicle resulted in a decrease in the drag coefficient under all yaw angle circumstances compared to the reference model. The drag reduction impact was shown to be positively correlated with crosswind conditions, reaching a maximum of 7.33% at a crosswind angle of 12°. The side force coefficient increased by 8% as the angle of attack reached 4°. The graph depicted in Fig. 9(c) illustrates the fluctuation of

Table 6 Experimental results of roll moment coefficient and the yaw moment coefficient at re = 5.1×10^6

	Moment coefficients					
Angle (°deg)	$C_{Mroll_{baseline}}$	$C_{Mroll_{modified}}$	**Reduction**	$C_{Myaw_{baseline}}$	$C_{Myaw_{modified}}$	**Reduction**
0	0.0051	0.0043	15.62%	0.0125	0.0171	-36.93%
2	0.0194	0.0208	-6.79%	0.0394	0.0474	-20.34%
4	0.0441	0.0409	7.10%	0.0848	0.0891	-5.02%
6	0.0690	0.0651	5.54%	0.1337	0.1380	-3.26%
8	0.0894	0.0854	4.46%	0.1639	0.1732	-5.69%
10	0.1108	0.1071	3.33%	0.1975	0.2073	-4.97%
12	0.1278	0.1166	8.70%	0.2206	0.2249	-1.92%

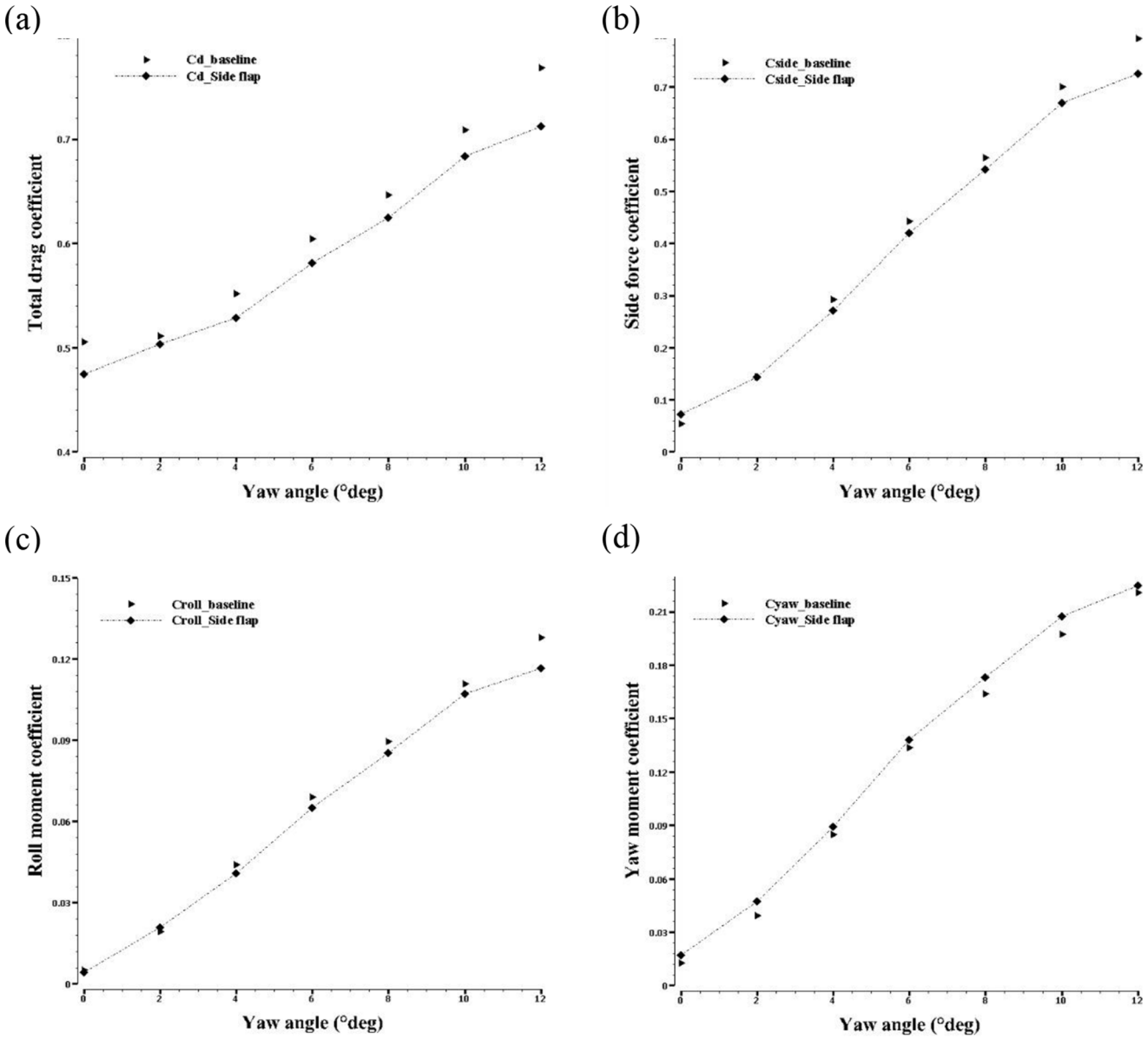

Fig. 9 Plot of (**a**) the total drag coefficient, (**b**) the side force coefficient, (**c**) the roll moment coefficient and (**d**) the yaw moment coefficient versus the yaw angles

the rolling moment. By including the side flap, the rolling moment coefficient is decreased for φ values greater than 4°. The peak was attained at φ = 12°. The side flap has a predominantly discernible impact at elevated yaw angles. These findings suggest that installing the side flap enhances the driving stability of automobiles.

4.3 Computational Fluid Dynamics Analysis on Crosswind

Figure 10 represents the graphs of drag coefficient and the side force coefficient versus the yaw angles, both numerical and experimental. Regarding the drag coefficient, the experimental values are slightly higher than the numerical ones. However, the increasing rate is the same for both. For the side force coefficient, the results match for the small angles and slightly differ as the yaw angle increases.

To better explore the mechanism of side flap attachment, the velocity fields behind the vehicle model were recovered from the numerical simulation. This was done in order to further illustrate the mechanism. Figures 11 and 12 depict the horizontal velocity streamlines surrounding the vehicle at three distinct yaw angles, namely at z = 0.02 and z = 0.06, respectively. The impact of the side flap is readily apparent in the flow patterns. The wake region, characterized by two primary vortices, is seen to be substantial and has significant influence over the rear portion. As the yaw angle increases, one vortex expands more than the other, resulting in the loss of symmetry in the wake region. The inclusion of the side flap has a direct impact on the wake, since it weakens the vortices and reduces the size of the area. As the yaw angle increases, the side flap is observed to diminish the strength of the vortices and lose their momentum, particularly the smaller vortex. This pertains to the decrease in the various forces mentioned in the outcome Tables 4 and 5.

Figure 13 illustrates the pressure distribution at the rear of the vehicle for both 0° and 12° yaw angles. The pressure contours are displayed for both the original and the altered model. Evidence demonstrates that the presence of a side flap diminishes the strength of the vortices and amplifies the pressure in the corresponding area. At a yaw angle of 0°, the pressure reading was around −146 Pa. However, when the side flap was introduced, the pressure increased to -120 Pa. At yaw angle of 12°, the pressure for the huge vortex increases from −200 Pa to -171 Pa. Moreover, the asymmetry of the wake area in relation to the yawing is demonstrated. Figure 14 presents a depiction of the pressure distribution at various locations behind the model, both for the baseline and modified models. Upon examination of the different yaw angles, it becomes evident that there is a phenomenon of pressure recovery, which elucidates the achieved reduction in drag during crosswind conditions. Additionally, it is also apparent that there exists dissimilarity in the vortices present behind the model when subjected to a yaw angle.

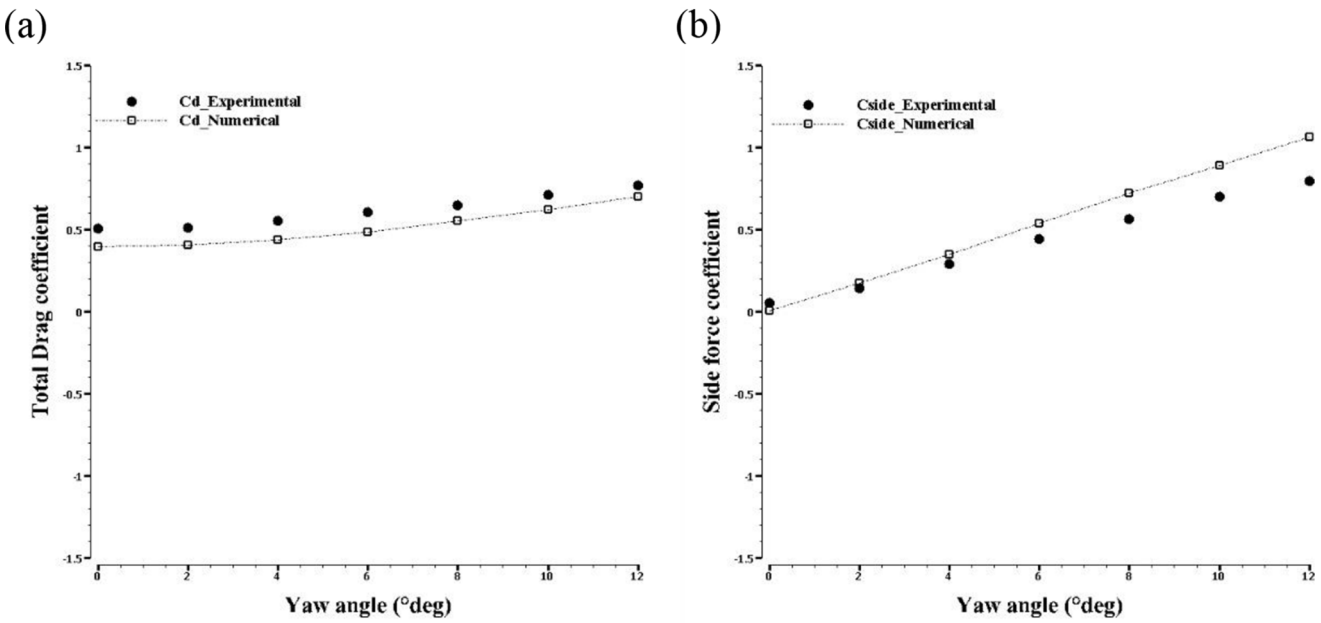

Fig. 10 Plot of (**a**) the total drag coefficient and (**b**) the side force coefficient versus the yaw angles for the numerical and experimental results

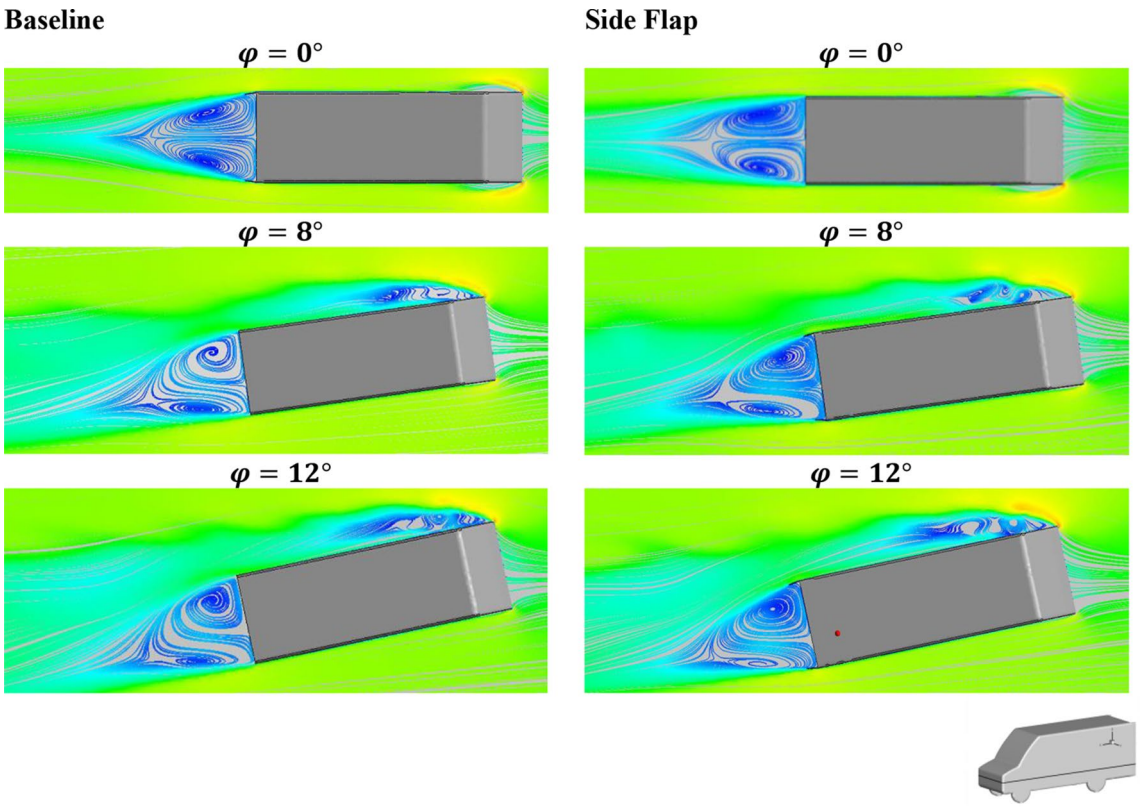

Fig. 11 Horizontal-plane velocity streamlines over the body for both the baseline and the modified model at different yaw angles (z = 0.02 m)

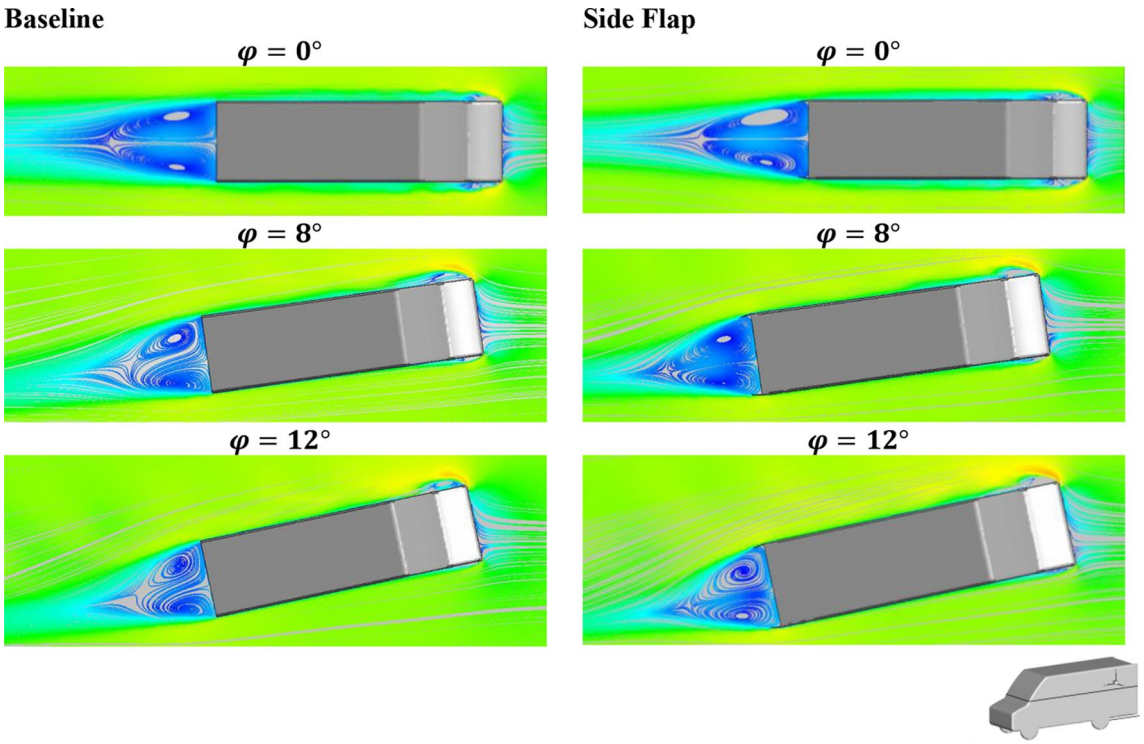

Fig. 12 Horizontal-plane velocity streamlines over the body for both the baseline and the modified model at different yaw angles (z = 0.06 m)

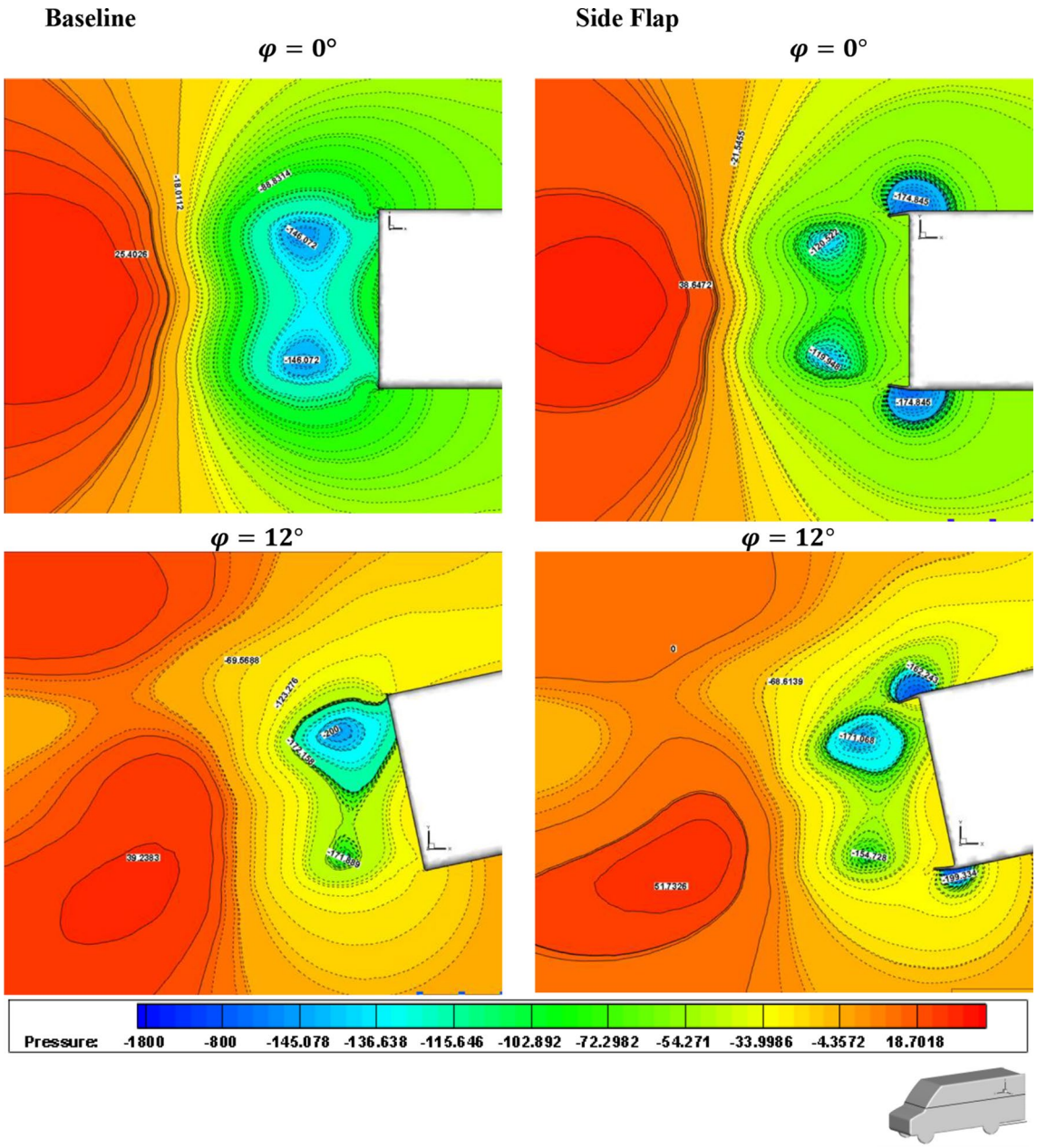

Fig. 13 Horizontal-plane pressure contours around the rear zone of the body for both the baseline and the modified model at different yaw angles (z = 0.05 m)

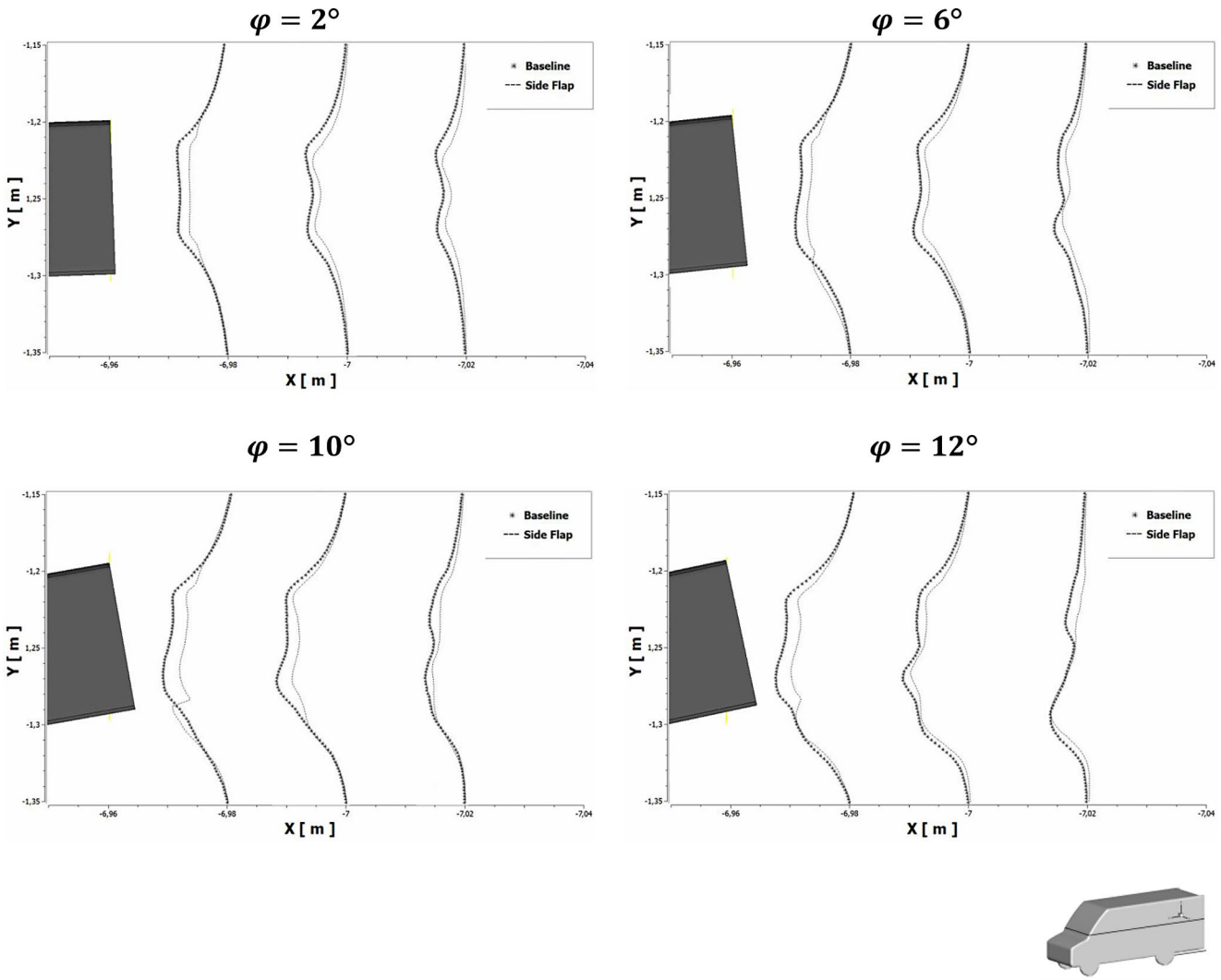

Fig. 14 Pressure distribution at various sections behind the van model for both the baseline and the side flap implemented (z = 0.06 m)

5 Conclusions

The present work assessed the impact of including a side flap as a passive flow control mechanism, utilizing both experimental and computational methods. The vehicle model is reduced in size to a scale of 1/28. The experiments were carried out in a wind tunnel operating at speed of 30 m/s ($Re = 5.1 \times 10^6$). The aerodynamic forces and moments were measured using a six-component force balance. Six configurations of the side flap were evaluated, and the optimal angle was found to be 10° which demonstrated a maximum decrease in drag of 6%. The numerical results closely matched the experimental data, exhibiting the same decrease rate. The stability of the model equipped with the side flap in the presence of crosswind was also examined and assessed. The inclusion of the side flap attachment has had a notable impact on the drag force, side force, and roll moment. With the side flap, the side force coefficient and the roll moment coefficient was reduced by 8.48% and 8.70% at a yaw angle φ = 12°, respectively. A smaller reduction is observed for the other yaw angles. The suggested side flap has been determined to efficiently manage the turbulent airflow in the wake region of the vehicle. It may be utilized to enhance the aerodynamic efficiency of high-speed transportation vehicles. The side flap may be integrated into the current vans and road transport vehicles utilized across various sectors, ranging from ambulatory services to freight transportation, serving as a straightforward auxiliary apparatus aimed at enhancing fuel efficiency as well as buses and heavy-duty vehicles. Additional research may be undertaken to thoroughly examine its influence on full-sized vehicles in conjunction with other mechanisms for regulating the yaw moment.

Acknowledgements This work is supported by the International University of Rabat (UIR). The authors express their gratitude to the Aerodynamic Laboratory of the International Islamic University of

Malaysia (IIUM) for granting them access to the wind tunnel facilities. They also extend their thanks to the LERMA laboratory for providing the in-house computing resources.

Author Contributions Fatima-Zahra Hachimy contributed to the design of the project, conducted both numerical and experimental work, performed data analysis and interpretation, and was responsible for drafting the article.Mohamed Aldheeb focused on the experimental work, engaged in data analysis and interpretation, and participated in the revision of the article.Ashraf A. Omar provided overall supervision, contributed to the design of the project, conducted numerical work, performed data analysis and interpretation, and granted final approval for the publication version.Waqar Asrar oversaw the experimental work, engaged in data analysis and interpretation, and provided final approval for the publication version.

Data Availability No datasets were generated or analysed during the current study.

Declarations

Competing Interests The authors declare no competing interests.

References

Ali JSM, Amran MF, Mohamad NA (2022) Experimental study on the Effect of Boundary Layer Control on the aerodynamics characteristics of NACA 0021 Aerofoil. J Adv Res Fluid Mech Therm Sci 94:129–137. https://doi.org/10.37934/ARFMTS.94.1.129137

Altaf A, Omar AA, Asrar W (2014) Passive drag reduction of square back road vehicles. J Wind Eng Ind Aerodyn 134:30–43. https://doi.org/10.1016/j.jweia.2014.08.006

Altaf A, Omar AA, Asrar W (2022) Passive Drag reduction of the Square Back Truck body. Int J Automot Mech Eng 19

ANSYS-FLUENT ANSYS FLUENT 12.0 Theory Guide –4.5.2 Shear-Stress Transport (SST) - Model. https://www.afs.enea.it/project/neptunius/docs/fluent/html/th/node67.htm. Accessed 1 Feb 2023

Barlow J, Rae W, Pope A (1999) Low-speed wind tunnel testing

Cerutti JJ, Sardu C, Cafiero G, Iuso G (2020) Active flow control on a square-back road vehicle. Fluids 5. https://doi.org/10.3390/fluids5020055

Cheng S, Chin K, And SM (2019) Experimental study of yaw angle effect on the aerodynamic characteristics of a road vehicle fitted with a rear spoiler. J Wind Eng

Cooper K (1985) The effect of front-edge rounding and rear-edge shaping on the aerodynamic drag of bluff vehicles in ground proximity. JSTOR. https://doi.org/10.4271/850288

Ehsani M, Ahmadi A, Fadai D (2016) Modeling of vehicle fuel consumption and carbon dioxide emission in road transport. Renew Sustain energy, Elsevier

Hachimy F, Omar A, Elsayed O (2022) The Accuracy of the Numerical Solution in Predicting Ahmed Body Components drag coefficients. CFD Lett

Hachimy FZ, Omar A, Elsayed O, Bouchaala K (2023) Parametric optimization for van drag reduction using a side flap. https://doi.org/101177/09544070231164200. https://doi.org/10.1177/09544070231164200

Haque AU, Asrar W, Omar AA et al (2016) Comparison of data correction methods for blockage effects in semispan wing model testing. EPJ Web Conf 114:02129. https://doi.org/10.1051/EPJCONF/201611402129

Hassan S, Islam T, Ali M et al Numerical study on aerodynamic drag reduction of racing cars. Elsevier

Heinemann T, Springer M, Lienhart H et al (2014) Active flow control on a 1:4 car model. Exp Fluids 55. https://doi.org/10.1007/s00348-014-1738-0

Howell J, Passmore M, Tuplin S (2013) Aerodynamic drag reduction on a simple Car-like shape with Rear Upper Body Taper. SAE Int J Passeng Cars - Mech Syst 6:52–60. https://doi.org/10.4271/2013-01-0462

Hucho WH, Sovran G (1993) Aerodynamics of road vehicles. Annu Rev Fluid Mech 25:485–537. https://doi.org/10.1146/annurev.fl.25.010193.002413

Hwang B, Lee S, Lee E et al (2016) Reduction of drag in heavy vehicles with two different types of advanced side skirts. J Wind Eng Ind Aerodyn 155:36–46

Hyams D, Sreenivas K, … RP- (2011) Computational simulation of model and full scale class 8 trucks with drag reduction devices. Comput Fluids, Elsevier

Jahanmiri M, Abbaspour M (2011) Experimental investigation of drag reduction on ahmed model using a combination of active flow control methods. IJE Trans Basics. https://doi.org/10.5829/idosi.ije.2011.24.04a.09. 24:

Joseph P, Amandolese X, Fluids JA (2012) Drag reduction on the 25 slant angle Ahmed reference body using pulsed jets. Exp Fluids 52:1169–1185. https://doi.org/10.1007/s00348-011-1245-5

Kim JJ, Lee S, Kim M et al (2017) Salient drag reduction of a heavy vehicle using modified cab-roof fairings. J Wind Eng Ind Aerodyn 164:138–151. https://doi.org/10.1016/j.jweia.2017.02.015

Kourta A, Mechanics PG (2012) Impact of the automotive aerodynamic control on the economic issues. J Appl Fluid Mech. https://doi.org/10.36884/jafm.2.02.11871

KR Cooper (2003) Truck aerodynamics reborn-lessons from the past. SAE Trans

Kumar Shaw K, Kesarwani Y, Chakravarty P (2020) Study of Dimple Effect on aerodynamic drag characteristics of a Car. Prepr Int J Innov Res Sci Eng Technol. https://doi.org/10.13140/RG.2.2.28628.42888

Lazăr S (2021) Computerized dynamic fluid simulation (CFD) for measuring the influence of the cab deflector on the aerodynamics of trucks. J Res Innov Sustain Soc 3

Leuschen J, Cooper KR (2009) Summary of full-scale wind tunnel tests of aerodynamic drag-reducing devices for tractor-trailers. Aerodyn Heavy Veh II Truck Buses Trains 41:451–462. https://doi.org/10.1007/978-3-540-85070-0_41/COVER

Lorite-Díez M, Jiménez-González JI, Pastur L et al (2020) Drag reduction on a three-dimensional blunt body with different rear cavities under cross-wind conditions. J Wind Eng Ind Aerodyn

Mariotti A, Buresti G, Salvetti MV (2019) Separation delay through contoured transverse grooves on a 2D boat-tailed bluff body: effects on drag reduction and wake flow features. Eur J Mech B. Fluids 74:351–362. https://doi.org/10.1016/j.euromechflu.2018.09.009

Martini H, Bergqvist B, Hjelm L, Löfdahl L (2011) Aerodynamic effects of roof deflector and cab side extenders for truck-trailer combinations. SAE Tech Pap

Menter F, Kuntz M, Turbulence R (2003) Ten years of industrial experience with the SST turbulence model. Turbul heat mass Transf

Mestiri R, Ahmed-Bensoltane A, Keirsbulck L et al (2014) Active flow control at the rear end of a generic car model using steady blowing. J Appl Fluid Mech 7. https://doi.org/10.36884/jafm.7.04.21752ï

Mohammadi M, Taleghani SA (2012) Active flow control by dielectric barrier discharge to increase stall angle of a NACA0012 airfoil. Arab J Sci Eng 39:2363–2370. https://doi.org/10.1007/S13369-013-0772-1

Ponnusamy N, Science MK-T (2016) U (2016) Numerical and experimental investigations of drag force on scaled car model. Therm Sci 20:. https://doi.org/10.2298/TSCI16S4153P

Sadeghipour S, Showkat Ali SA, Liu X et al (2020) Control of flows around bluff bodies mediated by porous materials. Exp Therm Fluid Sci 114. https://doi.org/10.1016/j.expthermflusci.2020.110048

Somashekar V (2021) Comparative study on the prediction of aerodynamic characteristics of mini-unmanned aerial vehicle with turbulence models. Int J Aviat Aeronaut Aerosp 8(1), P.7.

Tian J, Zhang Y, Zhu H, Xiao H (2017a) Aerodynamic drag reduction and flow control of Ahmed body with flaps. Adv Mech Eng 9:2017. https://doi.org/10.1177/1687814017711390

Tian J, Zhang Y, Zhu H, Xiao H (2017b) Aerodynamic drag reduction and flow control of Ahmed body with flaps. Adv Mech Eng 9. https://doi.org/10.1177/1687814017711390

West G, Apelt C (1982) The effects of tunnel blockage and aspect ratio on the mean flow past a circular cylinder with Reynolds numbers between 104 and 105. J Fluid Mech

Wong S, SD-IJ of M 2016 undefined Simulation Study on Vehicle Drag Reduction by Surface Dimples. publications.waset.org

Wood RM (2004) Impact of advanced aerodynamic technology on transportation energy consumption. SAE Technical Papers. SAE International